JOURNAL OF PROPULSION AND POWER
Vol. 34, No. 1, January–February 2018

Neutral Ingestion Effects on Plume Properties of a Radio-Frequency Plasma Discharge

Natalie R. S. Caruso* and Mitchell L. R. Walker†
Georgia Institute of Technology, Atlanta, Georgia 30332

DOI: 10.2514/1.B36404

To enable comparison of thruster performance across different vacuum facilities, an understanding of the effect of operating pressure on plasma plume properties generated in a helicon ion thruster architecture is required. Plasma property measurements acquired at two different vacuum facility operating pressures are used to determine the effect of neutral ingestion on the operation of a replica of the Madison Helicon Experiment at low power. The ion velocity distribution function, electron temperature, ion number density, and plasma potential are measured along the thruster axis. Plasma plume property measurements made at the "high-pressure condition" (3.0×10^{-4} torr corrected for argon) are compared to values recorded at the "low-pressure condition" (1.2×10^{-5} torr corrected for argon) for thruster operation at ~100 W radio-frequency forward power, 340 G source region magnetic field strength, and 2 cm^3/min argon volumetric flow rate. Operation at the high-pressure condition has 31–79 V lower ion energy, 0.8–6.1 eV lower electron temperature, and $1.1–5.2 \times 10^{14}$ $ions/m^3$ higher ion number densities than operation at the low-pressure condition. Changes in collision frequency and ionization balance result from increased neutral ingestion at the higher operating pressure.

Nomenclature

A	=	thruster exit area, m^2
C	=	arbitrary constant
d_{LP}	=	diameter of planar probe tip of Langmuir probe, m
$E_{ion,max}$	=	maximum ion energy
e	=	elementary charge
I_e	=	electron current, A
I_{is}	=	ion saturation current, A
K_{iz}	=	ionization rate constant
k_b	=	Boltzmann constant
M_a	=	argon atomic mass, atomic mass units
m_a	=	argon mass, kg
n_e	=	electron number density, $electron/m^3$
n_i	=	ion number density, ion/m^3
n_n	=	neutral number density, $atom/m^3$
P_{argon}	=	partial pressure of argon, torr
$Q_{ingested}$	=	volumetric neutral ingestion rate, cm^3/min
T_e	=	electron temperature, eV
T_n	=	neutral atom temperature, K
$\overline{v_{beam}}$	=	beam velocity, m/s
V_f	=	floating potential, V
V_{mp}	=	most-probable voltage, V
$V_{mp,corr.}$	=	most-probable voltage corrected with plasma potential, V
V_p	=	plasma potential, V
V_{PB}	=	probe bias voltage, V
η_c	=	thruster exit plane conductance
λ	=	mean free path, m
ν	=	collision frequency, collision/s
σ	=	collisional cross section, m^2

I. Introduction

HELICON ion thrusters are high-density plasma sources capable of accelerating ions without biased electrodes. In addition, the plume exiting the helicon ion thruster is quasi-neutral in nature, making a cathode or alternative beam neutralizing device unnecessary [1]. The lack of lifetime-limiting electrodes in contact with the helicon plasma and the subsequent promise of longer thruster life as compared to traditional gridded ion thrusters has led to an interest in further developing helicon ion thruster technology [2].

Evaluation of helicon ion thruster performance is conducted in ground-based vacuum test facilities that lower the pressure in the testing environment to simulate conditions in space. Vacuum facilities vary in physical size, base pressure, and effective pumping speed. These variations necessitate the establishment of facility standards to enable better understanding and comparison of recorded thruster performance. Facility criteria for Hall effect thruster (HET) evaluation are in development [3], but there currently exists a void in literature dedicated to establishing facility conditions required for helicon ion thruster characterization.

One of the main differences between plume characterization of helicon ion thrusters and HETs in vacuum test facilities and operation in space is background gas pressure [4]. Assessing the level of impact of background pressure on helicon thruster operation provides motivation for this investigation. Current helicon ion thruster literature presents plasma property measurements and performance predictions recorded across a wide range of facility operating pressures and thruster-chamber configurations [5–10]. Unfortunately, the influence of operating pressure on plasma properties due to affiliated neutral ingestion is not considered, making performance comparison difficult across multiple ground-based testing facilities.

When evaluating the effects of neutral ingestion on HET performance, Randolph et al. [11] suggest a facility operating pressure no greater than 5.0×10^{-5} torr (Randolph's limit) for reliable performance evaluation. Randolph's limit is predicated on reducing the amount of previously expelled neutral propellant entrained by the thruster to less than 3% of the provided thruster mass flow rate. Although the percentage limit of ingested mass flow rate versus the mass flow rate provided to the thruster is not maintained in this work, Randolph's additional criterion of free molecular flow of neutral particles in a vacuum chamber for an electric propulsion device operating at ≤1 kW total power with an unimpeded exit plane associated with the 5.0×10^{-5} torr pressure limit provides the foundation for the operating pressures considered. Randolph's limit provides a basis for studying the effect of operating pressure on helicon ion thruster plasma properties.

Received 21 July 2016; revision received 22 February 2017; accepted for publication 23 February 2017; published online 18 May 2017.

*NRC Research Associate, Naval Research Laboratory; ncaruso@space.nrl.navy.mil.

†Associate Professor, Aerospace Engineering Department; mitchell.walker@ae.gatech.edu. Associate Fellow AIAA.

To quantify the effect of neutral ingestion on helicon ion thruster performance, plasma properties are measured at two different operating pressures corresponding to two different argon-neutral ingestion flow rates. The "high-pressure condition" has an operating pressure of 3.0×10^{-4} torr corrected for argon with an associated argon ingestion volumetric flow rate of 3.8 cm^3/min. The "low-pressure condition" has an operating pressure of 1.2×10^{-5} torr corrected for argon corresponding to a 0.8 cm^3/min argon ingestion volumetric flow rate.

Plasma properties considered include the ion velocity distribution function (IVDF) and the most-probable voltage recorded using a retarding potential analyzer (RPA), plasma potential measured using a radio frequency (RF) compensated emissive probe, and electron temperature and ion number density recorded using an RF-compensated, planar disc Langmuir probe for a replica of the Madison Helicon Experiment (MadHeX). These plasma properties are chosen due to their influence on calculated thrust values for magnetic nozzles [12,13], a common configuration for helicon ion thrusters. Changes in these plasma properties due to operating pressure will directly relate the effect of facility backpressure on anticipated performance values. The MadHeX architecture is chosen due to existing literature documenting its operation in all three RF coupling modes and associated plasma properties of concern in this work [14–16]. Comparison of plasma property values and behaviors recorded at each operating pressure provides insight into the effect of neutral ingestion on helicon ion thruster performance and the mechanisms responsible. Note that the MadHeX replica does not operate in helicon mode in this work. Although the magnitudes of the effects of neutral ingestion on helicon ion thruster operation depend on the RF coupling mode and corresponding plasma density, the mechanisms instigated by an increased flow of neutral particles such as changes in the ionization balance and the rate of charge-exchange collisions affecting plasma properties are still present. This study identifies interactions between a plasma plume generated in a helicon ion thruster architecture and ingested neutral particles that will affect performance.

II. Experimental Setup

A. Madison Helicon Experiment Replica

The MadHeX replica shown in Fig. 1 is a six-solenoid RF helicon plasma source with a maximum mirror ratio of 1.44 when operated at the thruster's maximum possible axial magnetic field strengths of 1000 G in the magnetic nozzle and 700 G in the source region. For this work, MadHeX replica characterization is conducted for an axial magnetic field strength of 340 G in the source region. The axial magnetic field strength decreases to less than 0.5 G by 66 mm downstream of the thruster exit plane for the 340 G source region magnetic field strength operating condition. The solenoid coils have 500 turns of copper wire each and are arranged at set distances along a 10-cm-diam Pyrex discharge chamber as detailed in [14–16]. RF power is deposited using a half-turn, double-helix antenna located 60 cm upstream of the thruster exit plane between the second and third solenoid coils. During thruster operation, the exit plane is located approximately 0.75 m radially away from the facility sidewall as shown in Fig. 2 and approximately 4.1 m from the rear facility wall or 3.5 m away from the graphite beam dump.

During operation, the MadHeX replica is fed high-purity (99.9995%) argon gas as a propellant using stainless-steel Swagelok lines with a 3 cm nylon hose connector at the Pyrex propellant inlet. All results presented are for an argon volumetric flow rate of 2 cm^3/min (0.059 mg/s of argon) regulated by an MKS 1179A mass flow controller with an uncertainty of approximately 4–7% [17].

The RF signal broadcasts from a solid-copper, half-turn double-helix antenna measuring 13 cm in diameter and 18 cm long positioned between the second and third solenoid coils. The antenna is wrapped in fiberglass tape to prevent direct electrical contact between the antenna and the plasma structure. A 13.56 MHz RF signal is provided by a Yaesu FT-540 HF transceiver and amplified by an ACOM2000A linear amplifier. The matching network is a custom Pi-type network with a standing wave ratio (SWR) recorded using an LP-100 wattmeter. The SWR is held below 1.05 for all results provided with an uncertainty of ± 1 W for RF forward power and ± 0.05 for SWR [18]. The RF signal is carried on RG-8/U shielded cables from the radio throughout the RF system to a grounded n-type coaxial feed through. RF power is carried to the antenna directly via a vacuum rated RG-395 shielded cable. A 1.510 dB matched-line loss at 13.56 MHz for SWRs less than 1.10 for the system described has been measured using a MFJ-269 SWR meter [18]. MadHeX replica operation for all results presented is at 100 ± 5 W forward RF power with a 340 G source region magnetic field strength.

B. Vacuum Test Facility 1

MadHeX replica operation is conducted inside of Vacuum Test Facility 1 (VTF-1) at the Georgia Institute of Technology. VTF-1 measures 7 m long and 4 m in diameter. The pressure in VTF-1 is measured by an externally mounted Agilent BA 571 hot filament ionization gauge controlled by an Agilent XGS-600 gauge controller with a pressure measurement uncertainty of $+20$ to -10% [19]. Operating pressures presented are corrected for argon gas. Probe positions are controlled using a two-axis Parker Daedal 406XR

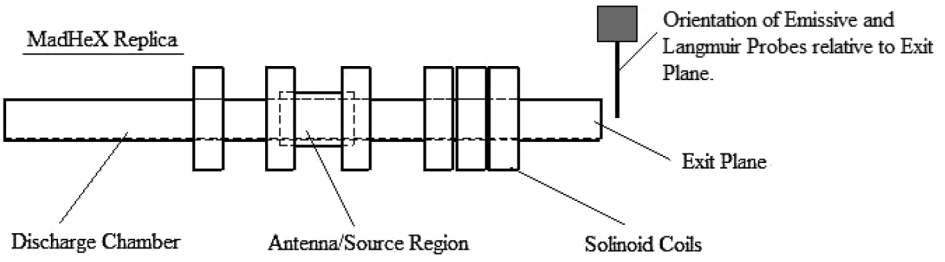

Fig. 1 Diagram of primary MadHeX replica components and orientation of emissive and Langmuir probes.

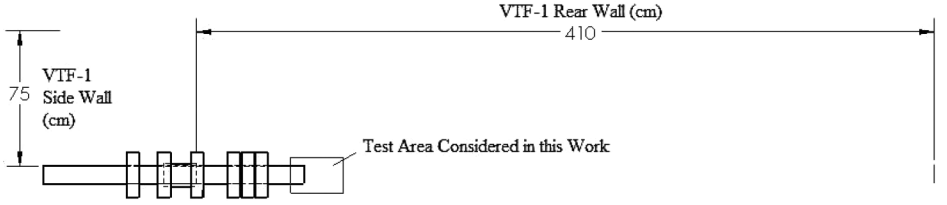

Fig. 2 Diagram of MadHeX replica orientation in Vacuum Test Facility 1. All measurements presented are recorded in the "test area" designated. Figure is to scale.

precision linear motion stage system with an uncertainty of ± 159 μm per motion stage.

To achieve either operating pressure condition, the chamber is evacuated to moderate vacuum (0.03 torr) by two 3800 cubic feet per minute (CFM) blowers and two 495 CFM rotary-vane pumps. To achieve the high-pressure condition (3×10^{-4} torr corrected for argon) from the 0.03 torr pressure environment, the CFM blowers and CFM rotary-vane pumps are shut down, and an Edwards STP-XA3203 turbomolecular pump with a pumping speed of 3200 l/s on nitrogen is engaged. An Edwards GV80 dry scroll pump provides vacuum line backpumping with a maximum pumping speed of 64.6 CFM for the turbomolecular pump.

To achieve the low-pressure condition (1.2×10^{-5} torr corrected for argon) from the 0.03 torr pressure environment, six NRC/CVC Varian HS48-95000 fractionating diffusion pumps with copper baffles chilled by three Polycold fast-cycle water vapor cryopumps running on HC 1100 refrigerant are engaged in conjunction with the CFM blowers and CFM rotary-vane pumps. The total configuration has a pumping speed of 125, 000 l/s on argon gas [20].

C. Radio-Frequency-Compensated Emissive Probe

Plasma potential is measured using an emitting, RF-compensated emissive probe. The overall probe measures 84 cm long with a thoriated-tungsten wire probe tip curved into a 0.127 mm diameter loop. The probe tip is fed through a 1.5-mm-diam, double-bore ceramic tube mounted to an RF compensation box. The compensation box holds two M-series ferrite toroids wrapped 25 times around with the signal wire to remove RF interference. Each choke provides 5600 Ω of impedance for a 13.56 MHz RF signal [20]. Probe orientation is perpendicular to the bulk plasma flow and perpendicular to the magnetic field as recommended in [21]. The plane of the tungsten probe tip loop is oriented parallel to the thruster exit plane permitting plasma flow through the loop as plasma exits the thruster [21].

Electron emission from the tungsten probe tip is controlled by dc current from a Xantrex XPD 60-9 power supply. A Keithley 2410 Sourcemeter biases the probe and records both the emitted and collected current at the probe tip. Collected probe tip current versus probe voltage bias is recorded using an Agilent 34970A data acquisition unit (DAQ). Plasma potential is determined from the collected I–V curves using the inflection point method as described in [22,23].

The uncertainty of the plasma potential calculated using the inflection point method is on the order of $\pm T_e/10$. Emissive probe tip heating inflates the resulting plasma potential due to the voltage drop across the probe circuit by 1 V. Power supply and total data collection instrument uncertainty is approximately 0.03% [24,25]. Error due to local regression (LOESS) smoothing falls within the error of the inflection point method and is considered negligible in comparison.

D. Retarding Potential Analyzer

The ion velocity distribution function (IVDF) is measured using a four-grid, U.S. Air Force Research Laboratory-designed RPA [26]. The RPA has four grids and a solid copper ion current collector. The order of the grids from plasma to collector is: floating, electron repulsion, ion repulsion, electron suppression, and a collector that is 0.8 mm thick and 3.15 cm in diameter [20]. All the RPA grids are composed of 316 stainless steel, 203 μm thick, and 3.15 cm in diameter. Each grid has a 31% transparency with aperture diameters of 229 μm arranged at a 394 μm pitch in a hexagonal hole pattern. The RPA is oriented along the centerline of the helicon ion thruster discharge chamber with the floating grid facing the open end of the helicon ion thruster. The chassis of the RPA remains electrically floating during data collection along with the floating front grid.

Ion current incident on the ion collection electrode is measured with a Keithley 6485 Picoammeter. The ion repulsion grid voltage is supplied by a Keithley 2410 Sourcemeter. The RPA collector plate current versus the ion repulsion grid voltage bias are collected by the DAQ. Before taking measurements at each thruster operating condition, the RPA bias scheme is optimized by adjusting the potential of the electron repulsion and electron suppression grids separately until maximum probe current is collected. Uncorrected most-probable voltage is the bias voltage corresponding to the maximum derivative of the I–V curve generated from the RPA collector current and ion repulsion grid bias voltage. Error in estimating most-probable voltage (uncorrected for plasma potential) for this analysis method is approximately $\pm 4\%$ [20]. Power supply and total data collection instrument uncertainty is less than 0.03% [24,25]. Error due to LOESS smoothing falls within the error of the analysis method and is considered negligible.

E. Radio-Frequency-Compensated Langmuir Probe

Electron temperature and ion number density are calculated from the I–V curve acquired by an RF-compensated Langmuir probe placed in the plasma. The Langmuir probe measures 84 cm long with a circular, planar tungsten probe tip 7.62 mm in diameter (d_{LP}). The RF compensation circuit is the same as the compensation circuit used for the RF-compensated emissive probe, with the exception of placing the m-series ferrite toroids in series on the signal line. The axis of the probe is oriented perpendicular to bulk propellant flow and perpendicular to the magnetic field with the plane of the probe tip disc parallel to the exit plane of the thruster as recommended in [23].

Electron temperature T_e (in electron volts) of the argon plasma is calculated via an exponential fit to the electron retardation region of the electron current curve. To increase the number of points available near the floating potential, the ion contribution to the total probe current is removed. Ion current is assumed proportional to the square root of the probe voltage and estimated using a linear fit [27]. Ion current is subtracted from the total probe current collected to generate curves of electron current as a function of probe voltage [28]. Equation (1) illustrates how electron temperature is determined using the derived exponential fit equation for electron current I_e versus the probe bias voltage V_{PB} as described in [29]. In the absence of a compensation electrode, the exponential fit is applied to the area of the electron retardation region closest to the floating potential and limited to only the most negative linear region in the log scale of the electron current–voltage trace to prevent overestimation of the electron temperature [28]. Using the calculated electron temperatures, Debye lengths are calculated for all the locations of interest in the plasma plume. The probe tip radius divided by the Debye length exceeds 10 for all cases, allowing ion number density to be estimated using the thin sheath regime [30]. The ion number density of the argon plasma is calculated using the probe tip diameter, electron temperature, and ion saturation current (I_{is}), as shown in Eq. (2) [31]. Ion saturation current is estimated as the average current collected between 5 and 50 V below the floating potential [30]. The uncertainty in the calculated electron temperatures using this method is ± 1eV for the low pressure condition and ± 0.2eV for the high-pressure condition; the uncertainty in the calculated ion number density is $\pm 50\%$ [30]:

$$I_e = C \exp\left(\frac{1}{T_e} V_{\mathrm{PB}}\right) \tag{1}$$

$$n_i = \frac{(4.3 \times 10^{15}) I_{\mathrm{is}}}{\sqrt{T_e} (d_{\mathrm{LP}})^2} \text{(for argon)} \tag{2}$$

Collected probe tip current versus probe tip voltage bias is measured using a Keithley 6485 Picoammeter. The probe tip voltage sweep ranges from −50 V up to 400 V, with varying dwell times altered per sweep to provide the best clarity of the knee behavior. Voltage is supplied by a Keithley 2410 Sourcemeter. The current and voltage values are collected by the DAQ. Power supply and total data collection instrument uncertainty is less than 0.03% [24,25].

III. Results

Plasma properties are measured along the main thruster axis from 79 mm upstream of the thruster exit plane to a maximum of 216 mm

downstream of the thruster exit plane. The exit plane represents a location of 0 mm, with locations upstream of the thruster exit plane represented by negative values and locations downstream of the exit plane represented by positive values. All results are presented for MadHeX replica operation at approximately 100 W forward RF power, 2 cm^3/min argon volumetric flow rate, and 340 G source region magnetic field strength. Both corrected and uncorrected most-probable voltage values are presented in this section due to the differences in measurement uncertainty. Corrected most-probable voltages have been adjusted by the corresponding measured plasma potential; uncorrected most-probable voltages are stated as recorded from the RPA *I–V* trace.

Figure 3 shows the IVDFs (uncorrected for plasma potential) at both pressure conditions. At the low-pressure condition, the IVDF most-probable voltages increase with downstream distance from the source region from 61 to 89 V over the full 145 mm range of interrogation as shown in Fig. 3 (left). The corrected most-probable voltages range from 33 V at the exit plane to 41 V at a distance of 16 mm downstream of the exit plane as shown in Fig. 4. The minimum corrected most-probable voltage of 21 V is reached at a distance of 66 mm downstream of the exit plane. The IVDFs for the high-pressure condition show a decrease in most-probable voltage from 29 V at a location 79 mm upstream of the thruster exit plane to 10 V at a location 66 mm downstream of the exit plane, as shown in Fig. 3 (right). Corrected most-probable voltages for the high-pressure condition decrease monotonically from 14 V at the thruster exit plane to 9 V at a distance of 66 mm downstream of the exit plane as shown in Fig. 4. Table 1 shows the differences in corrected and uncorrected most-probable voltages between the low-pressure and high-pressure conditions. The low-pressure condition corrected most-probable voltages are 12 V greater or more than the corresponding corrected most-probable voltages at the high-pressure condition.

Figure 5 shows the electron temperature recorded along the thruster centerline up to 216 mm downstream of the thruster exit plane for both pressure conditions. The electron temperature at the exit plane for the low-pressure condition is 5.6 eV higher than the corresponding electron temperature for the high-pressure condition.

Table 1 Differences between corrected and uncorrected most-probable voltages

Position, mm	−79	−34	0	16	66
$V_{mp,corr.}$, V	— —	— —	19	29	12
V_{mp}, V	31	54	63	70	79

Electron temperature decreases monotonically for both conditions to within a 1 eV difference in temperature by 166 mm downstream of the exit plane. The low-pressure condition maintains a higher temperature across the full distance considered. Both pressure cases have reached their final value (within error) by a distance of 116 mm from the thruster exit plane. The ion number density, shown in Fig. 6, is 4.5 times greater for the high-pressure condition than the low-pressure condition at the exit plane.

IV. Discussion

Differences in plasma property values and trends recorded at ∼100 W RF forward power and 340 G source region magnetic field strength at 2 cm^3/min argon volumetric flow rate are compared between both pressure conditions. Neutral ingestion is found to instigate changes in ion beam behavior, plume ionization rate, and ionization balance.

A. Ion Beam Behavior

In comparing the plasma properties for both pressure conditions, clear differences in ion energy are discernible between the accelerated ion populations. The high-pressure condition IVDFs are characterized by decreasing most-probable voltages with increasing distance downstream from the source region; this behavior is in stark contrast to the increasing most-probable voltages observed during operation at the low-pressure condition. The accelerated ion population at the low-pressure condition gains kinetic energy as ions are accelerated across the potential drop along the thruster main axis, resulting in increasing most-probable voltages correlating with

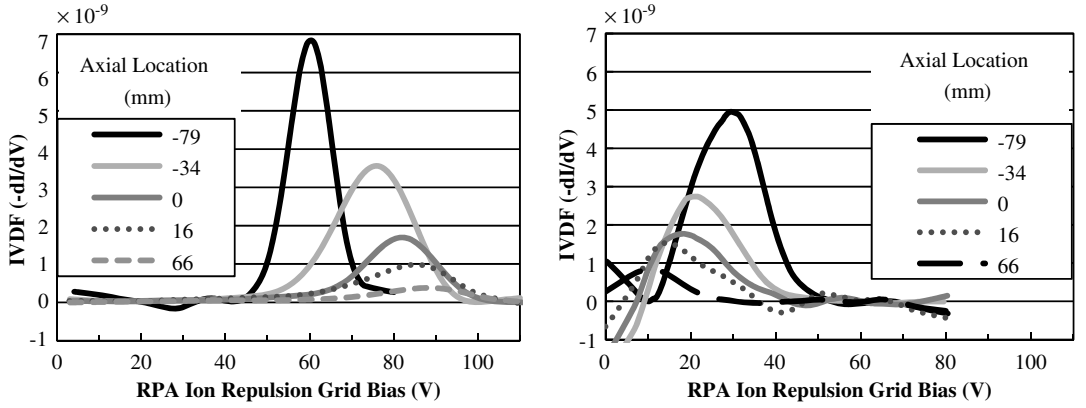

Fig. 3 IVDFs (uncorrected) recorded on thruster centerline at the low-pressure condition (left) and the high-pressure condition (right).

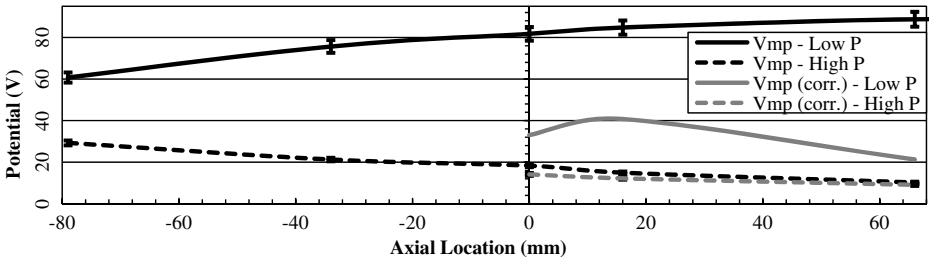

Fig. 4 Most-probable voltages V_{mp} and corrected most-probable voltages $V_{mp\ (corr.)}$ recorded on thruster centerline at the low-pressure condition ("Low P") and the high-pressure condition ("High P").

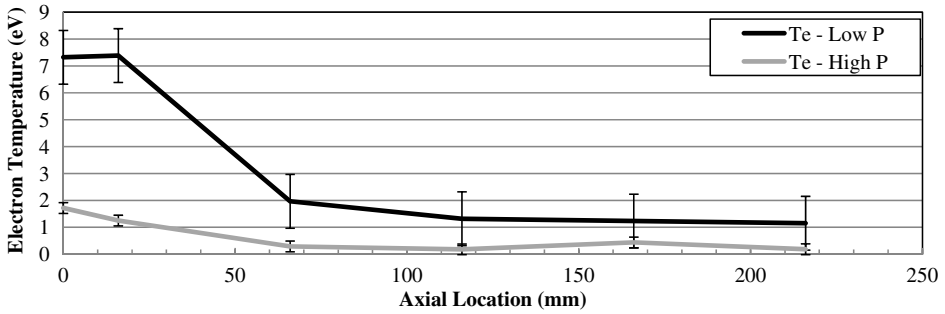

Fig. 5 Electron temperature recorded on thruster centerline at the low-pressure condition ("Low P") and the high-pressure condition ("High P").

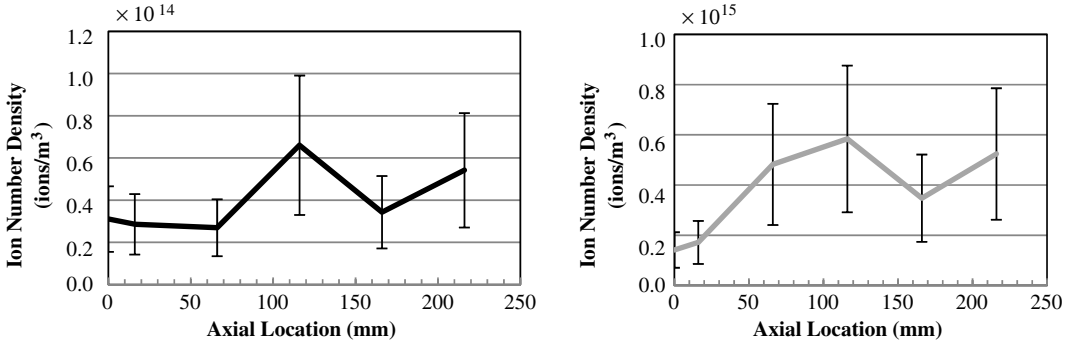

Fig. 6 Ion number density recorded on thruster centerline at the low-pressure condition (left) and the high-pressure condition (right).

increasing distance. The decreasing ion energy observed during operation at the high-pressure condition indicates energy losses in the accelerated ion population not observed at the low-pressure condition. The energy losses experienced at the high-pressure condition correlate with an increase in collisions between the accelerated ion population and other plume species. Note, the overall decrease in value of the most-probable voltages is related to the ionization balance discussed in Sec. IV.C.

Charge-exchange collisions and momentum-transfer collisions between the accelerated ions and other species located in the exhaust plume during operation at the high-pressure condition lead to the observed reduction in ion energy exhibited by the IVDFs in the downstream direction. The primary environmental difference between the two operating pressure conditions is the corresponding rates of neutral ingestion. The increase in neutral particle number density in the plume leads to an increase in energy-exchanging collisions between the accelerated ion population and neutral argon atoms. Using the recorded operating pressures from both pressure conditions, volumetric flow rates for ingested neutral argon atoms are calculated. The increase in neutral ingestion at the high-pressure condition leads to an increase in argon atoms available for collision with accelerated ions, leading to an increase in collision frequency, suspected to cause the observed reduction in ion energy along the thruster centerline in the downstream direction.

Neutral ingestion volumetric flow rates for both conditions are calculated using Eq. (3) and are displayed in Table 2. The neutral ingestion volumetric flow rate Q_{ingested} increases with the partial pressure of argon (P_{argon}), the area of the thruster (A), and the conductance of the thruster area (η_c). For the MadHeX replica, the exit plane area is 0.0079 m^2, and the conductance is assumed to be 1. Ingested neutral atom temperature T_N is assumed to be 298 K, and the mass of the argon propellant (M_a) is 39.948 AMU (atomic mass units):

$$Q_{\text{ingested}} = (7.82 \times 10^8)\frac{P_{\text{argon}} A \eta_c}{\sqrt{T_N M_a}} \tag{3}$$

The neutral ingestion volumetric flow rate is more than four times greater for the high-pressure condition at 3.8 cm^3/min argon than the 0.8 cm^3/min argon ingestion flow rate for the low-pressure condition. This large neutral population at the high-pressure condition will lead to an increase in collision frequency, resulting in greater energy transfer from the accelerated ions to the ingested argon neutrals.

Charge-exchange collisions are prevalent close to and downstream of the thruster exit plane and occur when a fast ion from the thruster ion beam collides with a neutral atom that has traveled into the exhaust plume [32]. This collision results in the formation of a slow ion and a fast neutral atom as shown in Eq. (4) and results in a reduction of ion energy [32]:

$$Ar^+_{(\text{fast})} + Ar_{(\text{slow})} \Rightarrow Ar_{(\text{fast})} + Ar^+_{(\text{slow})} \tag{4}$$

Momentum-exchange collisions also occur near the thruster exit plane, resulting in a transfer of energy from a high-energy, accelerated ion to any other colliding plume species. Momentum-exchange collisions with ingested neutrals are of particular interest because the net change in energy for the accelerated ion population would be negative. Ion-neutral collisions as a form of ion energy loss are more pervasive in a helicon ion thruster architecture at low power, when compared to other electric propulsion devices, due to the diffuse ion beam observed in this study. Unlike in HETs [32], the density at the edge of the exhaust plume structure in this work is not high enough to scatter incoming ingested atoms and thus prevent neutral atoms from traveling throughout the ion beam. IVDFs for the helicon ion thruster recorded at the high-pressure condition along the thruster centerline show that neutral ingestion occurs throughout the exhaust plume. The operation of helicon ion thrusters at higher power and in helicon coupling mode may generate plasma densities large

Table 2 Argon-neutral ingestion flow rates for both pressure conditions

Property	Low-pressure condition	High-pressure condition
P_{argon}, torr	1.4×10^{-5}	6.6×10^{-5}
n_n, atoms/m^3	4.54×10^{17} atoms/m^3	2.14×10^{18} atoms/m^3
Q_{ingested}, cm^3/min argon	0.8	3.8

Table 3 Mean free path lengths for charge-exchange collisions (λ_{CT}) and momentum-exchange collisions (λ_{MT})

Property	Low-pressure condition	High-pressure condition
λ_{CT}, m	3.15	0.67
λ_{MT}, m	2.20	0.47

enough to protect a highly ionized core. Higher plasma densities would relegate the impact of momentum and charge-exchange collisions to the fringes of the plume structure similar to HETs.

Mean free path lengths for both collision types are calculated using Eq. (5) for both pressure conditions. The mean free paths are presumed to start from the downstream edge of the MadHeX Replica's source region corresponding to the downstream edge of the RF antenna. A comparison of collision mean free paths between both pressure conditions is presented in Table 3 and illustrated in Fig. 7.

The mean free path is a function of the neutral number density (n_n) calculated using Eq. (6) and the collisional cross section σ. In this work, $\sigma = 7 \times 10^{-19}$ m^2 for argon ion energies up to 100 eV for charge-exchange collisions and $\sigma = 1 \times 10^{-18}$ m^2 for momentum-exchange collisions [33]. Neutral number density is a function of the partial pressure of argon from Table 2 and the ingested neutral temperature:

$$\lambda = \frac{1}{n_n \sigma} \tag{5}$$

$$n_n = \frac{P_{\text{argon}}}{k_b T_N} \tag{6}$$

Mean free path lengths for both charge-exchange collisions and momentum-transfer collisions for the low-pressure condition indicate that both collision types occur far downstream of the thruster exit. Mean free paths for the high-pressure condition, however, are of similar length as the distance between the source region and the thruster exit plane. Momentum-transfer collisions occur approximately 13 cm upstream of the thruster exit plane, whereas charge-exchange collisions occur approximately 7 cm downstream of the thruster exit. Collisions between accelerated ions and ingested neutrals lead to the decrease in ion energies observed at the high-pressure condition.

An examination of the collision frequency of both collision types of interest is conducted for the high-pressure condition. Collision frequency ν shown in Eq. (7) is a function of the ion beam velocity ($\overline{v_{\text{beam}}}$) calculated using Eq. (8) and the corresponding mean free path λ. Argon mass in Eq. (8) is in kilograms. Results are presented in Table 4. Beam velocity for both pressure conditions is presented in Table 5:

$$\nu = \frac{\overline{v_{\text{beam}}}}{\lambda} \tag{7}$$

$$\overline{v_{\text{beam}}} = \sqrt{\frac{2e(V_{\text{mp}} - V_p)}{m_{\text{argon}}}} \tag{8}$$

Collision frequencies at the high-pressure condition are highest close to the exit plane, where the beam velocity is also at its highest. Momentum-exchange collisions occur at a greater frequency than charge-exchange collisions, but results suggest that both collision types contribute to the reduction in ion velocity observed at the high-pressure condition as ions travel downstream along the thruster centerline. Inversely, ion velocity at the low-pressure condition increases as ions are accelerated across the potential gap moving downstream along the thruster centerline.

The observed reduction in ion energy at the high-pressure condition, as evident by the decreasing most-probable voltages of the IVDFs as ions travel downstream, results from an increased collision rate between the accelerated ion population and neutral argon atoms. The high-pressure condition has an ingested argon volumetric flow rate of 3.8 cm^3/min compared to the 0.8 cm^3/min ingested flow rate at the low-pressure condition, leading to an order of magnitude increase in argon-neutral number density. The increase in the population of argon atoms in the plume results in an increase of charge-exchange and momentum-exchange collisions rates between the accelerated ions and the neutral argon atoms. Although momentum-exchange collisions are more prevalent, both collision types lead to the reduction in ion energy at the high-pressure condition, as observed in the downstream direction along the thruster centerline.

The ion velocity behavior shown in Table 5 also reconciles the absence of significant ion number density changes along the thruster centerline, downstream of the exit plane. Treating the Langmuir probe as an ion flux probe, ion current collected is a function of ion number density and velocity. The increasing velocity of the ions at the low-pressure condition serves to yield consistent ion current despite a loss of ions due to scattering collisions as measurements are recorded at increasing downstream distances from the thruster exit plane. At the high-pressure condition, decreasing ion velocity coupled with an increase in charge-exchange collisions yields similar trends, resulting

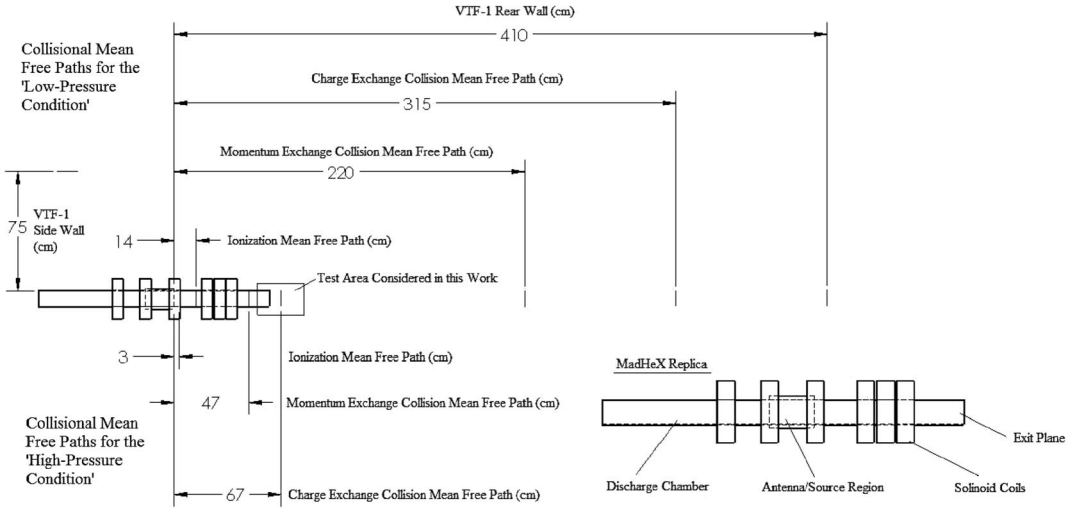

Fig. 7 Collisional mean free paths for both pressure conditions recorded for MadHeX Replica operation at ~100 W, 340 G, and 2 cm^3/min argon volumetric flow rate. Figure is to scale; measurements are in centimeters.

Table 4 Charge-exchange (ν_{CT}) and momentum-exchange (ν_{MT}) collision frequencies for the high-pressure condition

Distance from exit plane, mm	0	16	66
ν_{CT}, coll/s	12,383	11,507	9,918
ν_{MT}, coll/s	17,690	16,439	14,168

Table 5 Beam velocity for both pressure conditions

Distance from exit plane, mm	0	16	66
$\overline{v_{beam}}$ (high pressure), m/s	8,267	7,683	6,622
$\overline{v_{beam}}$ (low pressure), m/s	8,996	7,855	14,544

Table 6 Plume neutral ionization mean free paths and ion production rates at exit

Property	Low-pressure condition	High-pressure condition
λ_i, m	402	11,500
$(dn_i/dt)/(\text{ions/s m}^3)$	1.2×10^{17}	1.0×10^{15}

in a fluctuating but overall consistent ion current measurement across the range considered.

B. Plume Ionization

Although ion-neutral collisions explain the difference in ion energy behavior between the two pressure conditions, they do not account for the overall increase in ion number density at the high-pressure condition as illustrated in Fig. 6. Greater ion number density at the high-pressure condition may result from increased ionization in the source region or from a second neutral-plume interaction, where ingested neutral atoms become ionized as a result of collisions with hot plume electrons. This section examines the likelihood of the latter.

Slow ion formation may occur at both pressure conditions. These newly formed ions may then proceed to accelerate across the same potential drop near the thruster exit as the accelerated beam ions. Ion production rates are calculated to determine the rate of plume ionization. Ion production rates for both pressure conditions are calculated using Eq. (9); results are presented in Table 6. For these calculations, electron number density (n_e) is assumed to be equal to the ion number density (n_i) accounting for only singly-charged ions in the exhaust plume. The argon ionization rate constant K_{iz} is from the ionization curve of Fig. 3.16 in [34]. Ionization rates at the exit plane are 3.2×10^{-18} and 8.8×10^{-15} for the high-pressure and low-pressure conditions, respectively:

$$\frac{dn_i}{dt} = n_e n_n K_{iz} \tag{9}$$

Although ion production rates in the exhaust plume are on the same order of magnitude as the ion number densities observed at both pressure conditions, the large mean free paths suggest that ionization of plume neutrals is not prevalent at either pressure condition. Plume ionization is most likely not responsible for the observed increases in ion number density along the thruster centerline at either pressure condition or the overall larger ion number density observed at the high-pressure condition.

C. Electron Temperature and Ionization Balance

Examination of the final plasma property affected by increased neutral number density in the plume reveals changes in the ionization balance at higher neutral pressures. The electron temperature at the high-pressure condition is consistently lower than the corresponding electron temperature for the low-pressure condition as illustrated in Fig. 5. An increase in the argon partial pressure will cause a reduction in electron temperature due to changes in the ionization balance [35]. The increase in argon-neutral ingestion will cause an increase in argon-neutral partial pressure inside the thruster, leading to the recorded lower electron temperatures. A comparison of the ratios of ion energy to electron temperature at the exit plane for both pressure conditions are shown in Table 7 calculated using Eq. (10). The ratio of ion energy to electron temperature remains constant despite increasing argon-neutral pressure, indicating that changes in the ionization balance due to higher neutral flows are responsible for the overall reduction in ion energy and electron temperature from the low-pressure condition to the high-pressure condition [36]. In addition, the constant energy ratio indicates that electron cooling is not a predominant effect [36]:

Table 7 Ratio of ion energy over electron temperature at the exit plane

Property	Low-pressure condition	High-pressure condition
$E_{ion,Max}/T_e$	11.2	10.7

$$\text{Ratio} = \frac{E_{ion,Max}}{T_e} \tag{10}$$

D. Neutral Ingestion Effects

A comparison of plume behavior between both pressure conditions shows that changes in ion-neutral collision frequency and ionization balance occur at higher operating pressures corresponding with higher neutral ingestion rates. In this work, these behaviors lead to reductions in ion energy of 31 V up to 79 V, reductions in electron temperature of 0.8 eV up to 6.1 eV, and increases in ion number density of 1.1×10^{14} ions/m^3 up to 5.2×10^{14} ions/m^3 at the high-pressure condition. RF plasma discharges generated in a helicon ion thruster architecture evaluated at higher operating pressures and operating at low power have lower ion energies, lower electron temperatures, and higher ion number densities than those tested at lower operating pressures more closely resembling a spacelike environment. Performance values calculated from plasma plume properties of low-power, helicon ion thrusters tested at operating pressures in the 10^{-4} torr range are not repeatable at lower operating pressures.

V. Conclusions

The effects of neutral ingestion on plasma plume properties for radio frequency plasma discharges generated in a helicon ion thruster architecture result in reduced ion energy along the thruster centerline downstream of the exit plane, reduced overall electron temperature, and increased overall ion number density. Collisions between accelerated ions and ingested neutral atoms occur at greater rates for higher volumetric ingested flow rates, leading to losses in ion energy along the thruster centerline at the high-pressure condition. The increased neutral population at the high-pressure condition also leads to changes in ionization balance, resulting in lower electron temperatures and ion energies overall. Additional study of helicon ion thruster plume properties at facility operating pressures below 10^{-5} torr is required to determine a facility operating pressure limit suitable for evaluating low-power, helicon ion thruster performance.

Acknowledgments

The authors would like to thank Samuel Langendorf, Aaron Schinder, and Jonathan Walker for their help with the diagnostics and data collection. The authors also extend their gratitude to Jason Frieman who was heavily involved in the preliminary experiments of the MadHeX replica. This experimental research is supported by the U.S. Air Force Office of Scientific Research through grant FA9550-10-1-0396.

References

[1] Pottinger, S., Lappas, V., Charles, C., and Boswell, R., "Performance Characterization of a Helicon Double Layer Thruster Using Direct Thrust Measurements," *Journal of Physics D: Applied Physics*, Vol. 44, No. 23, 2011, Paper 235201. doi:10.1088/0022-3727/44/23/235201

[2] Charles, C., "Plasmas for Spacecraft Propulsion," *Journal of Physics D: Applied Physics*, Vol. 42, No. 16, 2009, Paper 163001. doi:10.1088/0022-3727/42/16/163001

[3] Semenkin, A., Kim, V., Gorshkov, O., and Jankovsky, R., "Development of Electric Propulsion Standards-Current Status and Further Activity," *Proceedings of the 27th International Electric Propulsion Conference*, Electric Rocket Propulsion Soc. (ERPS), IEPC Paper 2001-070, Pasadena, CA, 2001.

[4] Goebel, D., and Katz, I., *Fundamentals of Electric Propulsion: Ion and Hall Thrusters*, Wiley, Hoboken, NJ, 2008, pp. 32–36. doi:10.1002/9780470436448

[5] West, M. D., Charles, C., and Boswell, R. W., "Testing a Helicon Double Layer Thruster Immersed in a Space-Simulation Chamber," *Journal of Propulsion and Power*, Vol. 24, No. 1, 2008, pp. 134–141. doi:10.2514/1.31414

[6] Harle, T., Pottinger, S. J., Lappas, V. J., Charles, C., Boswell, R. W., and Perren, M., "Thrust Measurements of a Small Scale Helicon Double Layer Thruster," *Proceedings of the 32nd International Electric Propulsion Conference*, Electric Rocket Propulsion Soc. (ERPS), IEPC Paper 2011-103, Wiesbaden, Germany, 2011.

[7] Trezzolani, F., Lucca Fabris, A., Pavarin, D., Selmo, A., Tsaglov, A. I., Loyan, A. V., Rubalov, O. P., and Manente, M., "Low Power Radio-Frequency Plasma Thruster Development and Testing," *Proceedings of the 33rd International Electric Propulsion Conference*, Electric Rocket Propulsion Soc. (ERPS), IEPC Paper 2013-153, Washington, D.C., 2013.

[8] Takahashi, K., Komuro, A., and Anodo, A., "Effect of Source Diameter on Helicon Plasma Thruster Performance and Its High Power Operation," *Plasma Sources Science and Technology*, Vol. 24, No. 5, 2015, Paper 055004. doi:10.1088/0963-0252/24/5/055004

[9] Takahashi, K., Charles, C., Boswell, R., and Anodo, A., "Performance Improvement of a Permanent Magnet Helicon Plasma Thruster," *Journal of Physics D: Applied Physics*, Vol. 46, No. 35, 2013, Paper 352001. doi:10.1088/0022-3727/46/35/352001

[10] Faust, A., and Sedwick, R., "Performance of a Helicon Thruster Using Helium, Argon, and Water Vapor," *52nd Aerospace Sciences Meeting*, AIAA Paper 2014-0141, 2014.

[11] Randolph, T., Kim, V., Kaufman, H., Kozubsky, K., Zhurin, V., and Day, M., "Facility Effects on SPT Thruster Testing," *Proceedings of the 23rd International Electric Propulsion Conference*, Electric Rocket Propulsion Soc. (ERPS), IEPC Paper 1993-93, Seattle, WA, 1993.

[12] Takahashi, K., Charles, C., Boswell, R., and Ando, A., "Effect of Magnetic and Physical Nozzles on Plasma Thruster Performance," *Plasma Sources Science and Technology*, Vol. 23, No. 4, 2014, Paper 044004. doi:10.1088/0963-0252/23/4/044004

[13] Fruchtman, A., "The Thrust of a Collisional-Plasma Source," *IEEE Transactions on Plasma Science*, Vol. 39, No. 1, 2011, pp. 530–539. doi:10.1109/TPS.2010.2089067

[14] Wiebold, M., "The Effect of Radio-Frequency Self Bias on Ion Acceleration in Expanding Argon Plasmas in Helicon Sources," Ph.D. Dissertation, Electrical and Computer Engineering Dept., Univ. of Wisconsin–Madison, Madison, WI, 2011.

[15] Wiebold, M., Sung, Y., and Scharer, J. E., "Experimental Observation of Ion Beams in the Madison Helicon Experiment," *Physics of Plasmas*, Vol. 18, No. 6, 2011, Paper 063501. doi:10.1063/1.3596537

[16] Wiebold, M., Sung, Y., and Scharer, J. E., "Ion Acceleration in a Helicon Source Due to the Self-Bias Effect," *Physics of Plasmas*, Vol. 19, No. 5, 2012, Paper 053503. doi:10.1063/1.4714605

[17] Snyder, J. S., Baldwin, J., Frieman, J., Walker, M., Hicks, N., Polzin, K., and Singleton, J., "Flow Control and Measurement in Electric Propulsion Systems: Towards an AIAA Reference Standard," *Proceedings of the 33rd International Electric Propulsion Conference*, Electric Rocket Propulsion Soc. (ERPS), IEPC Paper 2013-425, Washington, D.C., 2013.

[18] Williams, L. T., and Walker, M. L. R., "Thrust Measurements of a RF Plasma Source," *Journal of Propulsion and Power*, Vol. 29, No. 3, 2013, pp. 520–527. doi:10.2514/1.B34574

[19] Tilford, C. R., "Sensitivity of Hot Cathode Ionization Gages," *Journal of Vacuum Science and Technology A*, Vol. 3, No. 3, 1985, pp. 546–550. doi:10.1116/1.572991

[20] Williams, L., "Ion Acceleration Mechanisms of Helicon Thrusters," Ph. D. Dissertation, Aerospace Engineering Dept., Georgia Inst. of Technology, Atlanta, GA, 2013.

[21] Lafleur, T., Charles, C., and Boswell, R. W., "Detailed Plasma Potential Measurements in a Radio Frequency Expanding Plasma Obtained from Various Electrostatic Probes," *Physics of Plasmas*, Vol. 16, No. 4, 2009, Paper 044510. doi:10.1063/1.3125314

[22] Sheehan, J. P., and Hershkowitz, N., "TOPICAL REVIEW: Emissive Probes," *Plasma Sources Science and Technology*, Vol. 20, No. 6, 2011, Paper 063001. doi:10.1088/0963-0252/20/6/063001

[23] Demidov, V. I., Ratynskaia, S. V., and Rypdal, K., "Electric Probes for Plasmas: The Link Between Theory and Instrument," *Review of Scientific Instruments*, Vol. 73, No. 10, 2002, pp. 3409–3439. doi:10.1063/1.1505099

[24] "User Manual for Keithley Sourcemeter, " Series 2400 Data Sheet, Keithley Instruments, p. 5, Keithley.com.

[25] "User Manual for Keithley Picoammeter, " Model 6485, Keithley Instruments, Cleveland, OH, 2001, p. A-2.

[26] Xu, K. G., "Ion Collimation and In-Channel Potential Shaping Using In-Channel Electrodes for Hall-Effect Thruster," Ph.D. Dissertation, Aerospace Engineering Dept., Georgia Inst. of Technology, Atlanta, GA, 2012.

[27] Chen, F., "Saturation Ion Currents to Langmuir Probes," *Journal of Applied Physics*, Vol. 36, No. 3, 1965, p. 675. doi:10.1063/1.1714200

[28] Sudit, D., and Chen, F., "RF Compensated Probes for High-Density Discharges," *Plasma Sources Science and Technology*, Vol. 3, No. 2, 1994, pp. 162–168. doi:10.1088/0963-0252/3/2/006

[29] Jameson, K., "Investigation of Hollow Cathode Effects on Total Thruster Efficiency in a 6 kW Hall Thruster," Ph.D. Dissertation, Aerospace Engineering Dept., Univ. of California, Los Angeles, CA, 2008.

[30] Reid, B.M., "The Influence of Neutral Flow Rate in the Operation of Hall Thrusters," Ph.D. Dissertation, Aerospace Engineering Dept., Univ. of Michigan, Ann Arbor, MI, 2009.

[31] Merlino, R., "Understanding Langmuir Probe Current-Voltage Characteristics," *American Journal of Physics*, Vol. 75, No. 12, 2007, pp. 1078–1085. doi:10.1119/1.2772282

[32] Crofton, M., and Boyd, I., "Momentum Modeling of a Hall Thruster Plume," *Proceedings of the 33rd International Electric Propulsion Conference*, Electric Rocket Propulsion Soc. (ERPS), IEPC Paper 2013-374, Washington, D.C., 2013.

[33] Phelps, A. V., "Cross Sections and Swarm Coefficients for Nitrogen Ions and Neutrals in N2 and Argon Ions and Neutrals in Ar for Energies from 0.1 eV to 10 keV," *Journal of Physical and Chemical Reference Data*, Vol. 20, No. 3, 1991, p. 557. doi:10.1063/1.555889

[34] Lieberman, M., and Lichtenberg, A., *Principles of Plasma Discharges and Materials Processing*, Wiley, Hoboken, NJ, 2005, p. 80. doi:10.1002/0471724254

[35] Takahashi, K., Charles, C., Boswell, R., Lieberman, M., and Hatakeyama, R., "Characterization of the Temperature of Free Electrons Diffusing from a Magnetically Expanding Current-Free Double Layer Plasma," *Journal of Physics D: Applied Physics*, Vol. 43, No. 16, 2010, Paper 185204. doi:10.1088/0022-3727/43/16/162001

[36] Lafleur, T., Cannat, F., Jarrige, J., Elias, P., and Packan, D., "Electron Dynamics and Ion Acceleration in Expanding-Plasma Thrusters," *Plasma Sources Science Technology*, Vol. 24, No. 6, 2015, Paper 065013. doi:10.1088/0963-0252/24/6/065013

J. Blandino
Associate Editor